Canadian Science Publishing | Canadian Journal of Civil Engineering

Experimental Investigation of 90^0 Intake Flow Patterns with and without Submerged Vanes under Sediment Feeding Conditions

Journal:	*Canadian Journal of Civil Engineering*
Manuscript ID	cjce-2020-0616.R2
Manuscript Type:	Article
Date Submitted by the Author:	14-Oct-2021
Complete List of Authors:	BOR, Asli; Izmir University of Economics, Department of Civil Engineering
Keyword:	Lateral intake, Turbulence, Submerged vanes, ADV, Separation zone
Is the invited manuscript for consideration in a Special Issue? :	Not applicable (regular submission)

Experimental Investigation of 90° Intake Flow Patterns with and without Submerged Vanes under Sediment Feeding Conditions

Aslı BOR

Department of Civil Engineering, Izmir University of Economics, Sakarya Cad. No:156, 35330, Balcova, Izmir, Turkey. Email: asli.turkben@ieu.edu.tr

ABSTRACT

In this study, two experiments were conducted in a 90° water intake to study 3D flow patterns and sediment distribution using submerged vanes under sediment feeding and live-bed conditions. One column three vanes were installed at a 20° angle maintaining for a water discharge ratio of $q_r \approx 0.1$. Three-dimensional mean and turbulent velocity components of flow in a 90° channel intake were measured by Acoustic Doppler Velocimetry (ADV). Flow characteristics of the intake structure area with no vanes are compared with those condition. Results showed that three vanes with single column reduced the amount of sediment by 20% in the intake diversion. In the downstream corner of the intake, high velocities were measured where scouring occurred. The vanes affected the intensity of secondary flow, turbulence energy, flow separation, and moved sediment deposition downstream of the main channel.

Author Keywords: Lateral intake; Turbulence; Submerged vanes; Separation zone; ADV

INTRODUCTION

Sediment transportation reduces reservoirs' life-span and hydrodynamic potential of dams and can contribute to the contamination of drinking water supplies (Elci et al. 2009). Another problem is that excessive deposition in front of the water intake structure can reduce the performance due to changes in the flow rate and even sediment entrance can cause turbine failure (Nakato et al. 1990; Wang et al. 1996; Barkdoll et al. 1995). Reducing the capacity of the intake structures affects design aims such as irrigation, flood control, power generation, and water supply. Consequently, the accuracy of the prediction of sediment deposition and scour is necessary in order to control sediment transport in river structures.

Mathematical and laboratory studies (Odgaard and Wang 1991a; Odgaard 2009; Odgaard and Wang 1991b; Barkdoll et al. 1999; Yang 2008; Herrero et al. 2015) showed that one recirculation area occurred before the lateral intake, in the inner side of the main channel with lower velocities (Zone (1) in Figure 1). This is the main deposition zone in the main channel inner wall and the sediments enter the intake channel from here (Herrero et al. 2015). In the main channel outer side, there is another recirculation area occurred opposite the intake (Zone (2) in Figure 1) depends on the width ratio between the main channel and the lateral branch (Barkdoll et al. 1999). From flow direction to upstream, part of the diversion, called a dividing stream surface, divides the water flow and enters the intake channel. There is significant scour zone at the mount of the intake corner at the downstream, and other at the main channel (Zone (3) in Figure 1). The separation zone is the low-velocity area along the intake entrance adjacent wall immediately upstream of the channel junction in which another recirculation zone occurs (Zone (4) in Figure 1). This zone is found to generate the deposition of a significant part of the sediment that enters the lateral branch (Bulle 1926). To reduce the amount of sediment entering the water intake structure, it is necessary to change the direction of the flow and introduce secondary circulation. There are several methods that can be applied in practice to control sediment transport. Periodic dredging is still the most common, but it is expensive. Submerged vanes application is a practical and more economical solution for controlling sediment transport. It is used in practice to improve riverbed morphology and riverbank erosion, as well. First, important parameters concerning the use of submerged vanes were introduced by Potapov and Pyshkin (1947). This subject remained untouched until 1980s by Odgaard and Kennedy (1983). They built a physical model of the Sacramento River bend in California, developed the analytical model, and compared the solutions. They saw submerged vanes significantly reduced the secondary circulation and the high velocity attack in the outer side. Comprehensive studies were conducted in the 1980s to understand flow and sediment behavior using submerged vanes. Submerged vanes change the magnitude and direction of bed shear stress, modifying the velocity and depth of the flow and change the sediment transport mechanism in the influenced area. The submerged vanes are installed with a suitable angle of inclination to the downstream direction of the main channel flow to produce a secondary current downstream of the main channel. Kasthuri and Pundarikanthan (1987) researched flow separation and vortex dimensions at the entrance of a 90° intake structure. They indicated that increasing diversion ratio could reduce the dimensions of the vortex area. They also concluded that the dimensions of the vortex area remained unchanged if the diversion ratio was greater than 0.7. Nakato et al. (1990) performed a case study for sediment control using submerged vanes at Iowa Powers Council Bluff Power Station. The bed level of the river was lowered due to the scour hole dimension and suspended sediment reduced water flow in the intake. Barkdoll et al. (1999) presented that when submerged vanes were placed at the entrance of the intake structure, their effectiveness decreased as the diversion ratio increased. Barkdoll (1997) observed the formation of a separation zone attached to the inner wall of the derivation and presented that the sediment transported to the derivation inlet and deposited in the flow separation zone, at the entrance of the diversion. In addition, Barkdoll et al. (1999) concluded that the separation region in the deflection decreases as the size discharge ratio q_r increases. They also showed that sediment enters the intake, if the diversion ratio was less than 0.2. There have been many laboratory studies for different vane angles to see the effect of submerged vane placement on sediment entry (Bajestan and Nazari 1999; Keshavarzi and Habibi 2005; Hassanpour et al. 2007; Abbasi and MalekNejad 2014; Amiri et al. 2013; Beygipoor et al. 2013). Davoodi and Bejestan (2012) investigated the optimum distance to install submerged vanes on trapezoidal channel. They found that when the distance between vanes was equal to $8H$, the sediment inflow to intake was minimum.

There are numerous studies about submerged vanes (Sruthi et al. 2017; Karami et al. 2017) to evaluating the impact of submerged vanes on amount of the sediments moving through the intake channel and the common feature is that all were conducted without sediment feeding. A set of more detailed data on prototype submerged vane performance such as intensity of secondary flow, turbulence energy, flow separation or sediment motion would provide additional definitive confirmation of the limits of vane use for sediment control (Barkdoll et al. 1999).

In this paper, two laboratory experiments have been performed to investigate erosion- deposition patterns and three-dimensional flow structure in front of a 90° intake channel. Sediment feeding was performed to protect the sediment mixture tissue during the experiment. This paper explains the effect of using the single column three vanes with 9 *cm* vane spacing for angles of attack 20° under sediment feeding conditions in mobile-bed channel. Particular emphasis was to observe the role of main channel bed topography, and its evolution under mobile bed conditions in a 90° intake, and submerged vanes influence on sediment transport at the equilibrium stage. Three-dimensional flow measurements were performed to define the formation of secondary flow patterns in the diversion entrance. Also bed change data were collected to determine the volume of sediments entering the entrance of the intake, around the vanes and to describe erosion and deposition zones. The bed topography data have been published previously by Bor (2018). Flow patterns and recirculation area in the intake flow separation zone were investigated. By comparing with and without vane conditions, the impact of the single column three vanes on bed topography and water flow in front of a diversion channel is presented.

METHODOLOGY

Experimental Setup and Experiments

Experiments were carried out in a recirculating phsical model located in the Instituto Superior Tecnico (IST) Hydraulics laboratory in Lisbon, with a 12 m long and 1 m wide rectangular concrete channel, with some parts composed of glass allowing the visualization, and 5 m long, 15 cm wide lateral intake that joined the main channel at the angle of 90°. The bottom slope of the main channel was 0.007. A schematic plan view of the model is displayed in Figure 2. The constant water discharge was pumped in the channel by a speed control unit with ±0.1 l/s accuracy located upstream. The rectangular basin and main water tank were located at the channel downstream. Sediment feeding was performed by using a sediment recovery system at the downstream end of the main channel consisting of a bottom outlet, sediment recovery tank and sediment container. A conveyor belt was used for sediment feeding in the inlet of the channel with a velocity regulator device.

Channel bed topography measured by a Mini-EchoSounder probe (UltraLab UWS) in channels with ±1 *mm* accuracy by topographic surveys. The water depths were measured by ultrasonic limnimeter with ±1 mm accuracy. The robotic arms instrumentation was installed on an automatic movable frame in X, Y and Z directions in the main and intake channel (Figure 3), and proceeded along the channel in order to record bed and water elevations simultaneously. During each experiment, 22 longitudinal bed elevation and water surface profiles laterally spaced by $\Delta Y = 4$ cm along the main channel were measured. At the same time, another robotic arm used to determine bed topography and water surface along the intake channel, was situated in the middle of the channel, which would move a distance of 50 cm. The sediment bed was flattened before each experiment test and and water is supplied gently without causing any disturbance to the bed material. The bed topography was recorded before the experiments for both main and intake channel.

The experiments were carried out under the mobile bed condition. At the beginning, the initial movable bed was prepared by using the same sediment mixtures and flattened before each experiment test. Then, the sediment container was filled, and pumps were started. The valve was slowly opened to allow a specified discharge. The backwater effects at the downstream end of the main channel were prevented by a tailgate. A uniform flow condition in the channel was achieved when the measured bed and water surface were parallel to each other. First, the main and intake channels were filled with water discharge, and then after adjusted to the required value, the suction pump installed at the downstream end of the water intake structure was opened for taking water inside it. After reaching the uniform flow condition, sediment was dropped manually at the upstream of the channel at a constant rate. Downstream tailgate was slowly lowered till the downstream water depth reaches 12 cm, corresponding to the approximation normal depth determined the Manning formula.

The tests were carried out until equilibrium conditions were reached. The equilibrium condition was defined as the state at which the outgoing sediment rate was equal to the incoming rate and the bed topography had attained a quasi-steady state (Guillén-Ludeña et al. 2017). The adjustment of the channel bed surface necessary to reach an equilibrium condition between the inflow sediment feeding rate and outflow rate is small. The amount of incoming sediment rates was determined by weighing the sediments collected in the sediment recovery tank at each time interval $\Delta t = 15h$. Water surface elevations and bed topography were recorded during the tests at $t = 1.5h$, $t = 9.0h$ and when equilibrium was reached. The equilibrium state was reached after 12 hours and tests were stopped at $t = 13.5$ hours. The Mini-EchoSounder probe needs to be slightly submerged in the water, so the downstream tailgate was slowly raised to increase the water level and decrease the flow velocity to avoid sediment movement. When the measurements were accomplished, discharge was reduced, and sediment feeding was switched off. While restarting the tests, discharge was adjusted to the set value, sediment feeding was switched on and the downstream tailgate was slowly lowered to a water depth of 12 cm again. After the tests, water was removed gently by controlling tailgate from the channels without distribution of the bed topography. The bed topography was fixed by spraying water while sieving cement powder and then the surface was varnished. The velocity measurements were conducted without sediment feeding. The velocities were measured by Acoustic-Doppler Velocimetry (ADV) in three directions (u_x, u_y, u_z) and recorded each point for 3 minutes.

EXPERIMENT PARAMETERS

The initial movable sediment bed was prepared with uniform sand with $d_{50} = 0.85$ mm median grain size and $\sigma = 1.35$ geometric standard deviation in 15 cm thickness for both the channel and intake. The flume bed was flattened and bed topography was measured before the experiment was started. Barkdoll et al. (1999) observed that sediment enters the intake when the discharge ratio is less than 0.2. According to this study, the flow discharges of the main and intake channel were $Q_m = 45$ l/s and $Q_i = 5$ l/s respectively and the selected discharge ratio was q_r, being ≈ 0.1. Sediment feeding rate was $Q_{sed-main} = 0.5$ kg/min for each test. The flow depth was maintained at, $d = 12$ cm in both tests. The average flow velocity $u_0 = Q/bd$ and the Froude number $F_r = u_0/(gd)^{0.5}$ at the upstream reach of the channel were 0.38 m/s and 0.28, respectively.

The position of the submerged vanes according to the water intake structure is shown in Figure 2. Before the studies started, a serious literature review had been conducted about submerged vanes and parameters such as number of submerged vanes, submerged vane height, length, vane angle of attack, vane spacing, and distance from bank to vane. In this study, single column three vanes were placed at angle $\alpha = 20^0$ to the main flow direction with dimensions of 3 cm high, 9 cm long and 10 mm thick with vane spacing $\delta_n = 3H$ and vane to bank distance $\delta_b = 5H$ according to recommendations of previous studies (Odgaard and Kennedy 1983; Odgaard and Wang 1991a,b; Barkdoll et al. 1999; Sruthi et al. 2017).

The three-component instantaneous flow velocities (u_x, u_y, u_z) in the main channel and intake were measured with a Nortek Acoustic-Doppler Velocimeter (ADV) (10 MHz) at a sampling frequency of 100 Hz. It consists of a central transmitter, surrounded by four receivers, placed in a water-filled column that is in contact with the water surface (Lemmin and Rolland 1997). In this study, velocity measurements were recorded in three directions (u_x, u_y, u_z) at each point for 3 minutes, and 18000 data was collected for each point. Compared to other studies in the literature, the number of data received is considered appropriate for a region where turbulent flow occurs (Biron et al. 1996; Weber et al. 2001). The velocimetry was placed in a robotic arm, and data sampling was controlled by a computer program. For each velocity component, the Phase-Space Threshold (PST) filter algorithm was used to clear the velocity time series from outliers. This method is based on the physical principle that maximum particle acceleration must have a certain maximum value (Goring and Nikora 2002). In the initial processing of the data, points with an average correlation of less than 70% or a SNR of less than 15 dB were discarded. ADV data post-processing code was written in MATLAB and consists of several independent functions. Flow patterns were obtained from time-averaging of velocity measurements after filtering of the velocity data. Figure 3 describes the measurement mesh points for flow velocities: it includes the horizontal axes x and y, directed in the stream-wise and spanwise directions, respectively. The vertical axis z starts at the bottom, and is directed towards the water surface in the without vane experiment, 3738 mesh points were used in the main channel, including 25 profiles in the X direction and 8 profiles in the Y direction with 5 cm vertical spacing, and in the with vane experiment 4260 mesh points were used including 33 profiles in X direction and 11 profiles in Y direction in the main channel with 5 cm vertical spacing. A total of 253 mesh points were used in the intake channel including 6 profiles in center-line.

RESULTS

Bed Topography

The bed topography was determined by using the data obtained form the Mini-EchoSounder and ultrasonic limnimeter from at the beginning of the tests till reaching equilibrium. At the beginning ($t = 0$ h), the bed was horizontal in the main and intake channels. The bed topography was recorded during the experiments at $t = 1.5$ h, at $t = 9.0$ h, and at equilibrium. The time to reach equilibrium varied after 13.5 hours for each test. During the tests, it was observed that maximum scour depth occurred at the mouth of the intake corner on the downstream side (Zone (3) in Figure 1). The temporal variation of maximum scour depth observations for with and without submerged vane experiments were compared in Zone (3), and graphical plots for this comparison are illustrated in Figure 4. The measured bed topographies are depicted in Figure 5 for all test cases. The figure shows that the scouring area was observed just downstream from the intake channel at the beginning of each experiment in both cases, i.e. with and without vanes. To provide a more detailed visualization, the bed profiles in $Y = 10$ cm, $Y = 30$ cm, and $Y = 50$ cm away from the inner side of the main channel and intake axis are shown in Figure 6 for both experiments. The view of the final topography in front of intake and around the vanes is depicted in Figure 7. The results show that the submerged vane decreased scour depth, and reduced the amount of sediment entering the intake channel. On the other hand, for both cases in the experiments, significant scour areas were observed in the downstream corner of the intake, and this scouring in the main channel was much more pronounced than in the intake channel. Similar results also obtained by (Barkdoll et al. 1995; Herrero et al. 2015)

Flow Patterns

Measurements of three-dimensional velocities u_x, u_y and u_z in the main and intake channels were conducted using Acoustic-Doppler Velocimetry (ADV) deployed with robotic arms at equilibrium state. All results were obtained by MATLAB and plotted after filtering the experimental data. The time-averaged components of the velocity vector were measured and normalized with the mean flow velocity at the upstream of the main channel ($U_m = 0.36$ m/s). Figure 8 shows the contour plots of $\bar{u}_{xy} = \sqrt{(\bar{u}/U)^2 + (\bar{v}/U)^2}$ with velocity vector plots of $\bar{u}$ and $\bar{v}$ at 5 cm above the bed presented by a color scheme on horizontal planes $Z = [6.5, 7.5, 10.5, 12]$ cm both for without vane and with vane experiments (U is the average approach flow velocity in the main and intake channel). Time averaged velocities $\bar{u}_{yz}$ with vertical velocity vector plots $\bar{v}$ and $\bar{w}$ at six measured cross sections, namely $X = [0, 20, 25, 45, 55, 85]$ cm, and intake cross section for channel width are presented in Figure 9, with water surface elevations and bed profiles. The time-averaged velocity components of the main channel are normalized by the mean flow velocity of $U_m = 0.36$ m/s. The variation of secondary flow circulation in the channel can be defined in Figure 9. The turbulence kinetic energy k $(cm^2 s^{-2})$ was calculated by using the three-dimensional velocity components as:

$$\text{k} = 0.5(\overline{u'u'} + \overline{v'v'} + \overline{w'w'}) \tag{1}$$

where; $u' = u - \bar{u}$, $v' = v - \bar{v}$, and $w' = w - \bar{w}$ are the fluctuating velocity components based on Reynolds decomposition, indicating the possible location of the shear layers within the intake shown in Figure 10.

DISCUSSION

Two flow structures were identified in the intake entrance; 1) separation zone starting at the upstream corner of the diversion channel and developing along the inner wall of the intake channel and recirculation flow zone associated with the separation zone indicated with low velocities (Zone (4)) 2) significant scour zone at the mount of the intake corner at the downstream indicated with high velocities (Zone (3)). The flow separation zone was reported also by (Barkdoll et al. 1999) and (Karami et al. 2017). When comparing the bed topography between both cases, i.e. with and without vane, the scour area gradually grew up because of a secondary flow in Zone (3). It is certain that the depth of the scour increased by the without vane case. Also, erosive capacity of the flow at the location of the intake increased with time. In the corner of the Zone (3), the bed level was deeper (∼ 14.5 cm) for without vane experiment than for with vane (10 cm). At the same time, because of the lower velocities observed in separation zone (Zone (4), Figure 1), in the other corner of upstream part of the intake, the sediment transport is increased, causing continuous flow of sediment into the intake channel. This increased the sediment transport capacity and also the bed slope. Maximum deposition of the sediment thickness in the intake channel is 6 cm without submerged vanes, whereas it decreased to 4 cm, after the with submerged vane experiment. The upstream from the diversion is called 'flow dividing surface', which separates the flow into two directions, into the intake channel, and into the main channel downstream. Two large recirculations occurred; one on the inner side of the main channel just before the intake, the other on the outer side of the main channel, opposite of the intake. It is clear that the without vane had higher the deposition values (6 cm) than the with vane (2 cm), for Zone (1), Zone (2) and Zone (4). Due to the lower velocities in Zone (4), it is easier to counter the centrifugal force and change the direction of the flow (Neary et al. 1999). Since it is slightly above the limit value of the flow intensity, $u/u_{cr} = 1.1$, no clear bed forms were observed at the the main channel bed, when equilibrium conditions was reached. In the without vane experiments, bed changes on the upstream side of the main channel started approximately $x > 1.5m$ above the intake structure. In the with vane experiments, the bed deformation started almost from the very beginning of the main channel. The bed deformations were completely different when the current came to the intake channel. The results were consistent with previous studies (Herrero et al. 2015; Bajestan and Nazari 1999; Sruthi et al. 2017; Karami et al. 2017). From Figure 6, slightly more erosion was found with vane experiment, along the center line of the intake when compared with the scour bed profile without vanes. There was very little effect on the bed profile along the center line of the main channel (Y = 50 cm) with vane experiment. It can be observed that submerged vanes reduced the amount of sediment entering the intake channel by as much as 20%. In addition, sediment transport in the main channel decreased by 125% under the mobile bed condition. Similar results was also reported in previous studies (Kasthuri and Pundarikanthan 1987; Nakato et al. 1990; Barkdoll et al. 1995; Wang et al. 1996; Odgaard and Spoljaric 1986; Barkdoll et al. 1999).

3D Flow Structure

The analysis of horizontal velocity distribution indicates that the effects of positive pressure gradient on the flow field. In all cases, flow accelerates in the downstream of the intake channel entrance (Zone (3)), causes scouring, decelerates in the inside of the intake with outer and inner side of the main channel, and causes deposition due to the stream-wise pressure gradients (Zone (1), Zone (2), Zone (4)). The diversion flow discharge provided by intake channel causes maximum velocity immediately at the mouth of the intake. As the flow enters the intake, a small erosion area is observed next to the outer wall of the intake, caused by the strength of the secondary flow increases. The vector arrows are generally directed toward the inner side near the main channel and inside of the intake. The secondary flow becomes more intense as the flow reaches intake corner, and the fast flow near the inner side of the main channel is carried beyond the inner side by the secondary flow (Figure 5 and Figure 8). It has been observed that the velocity component in the vertical direction (w) is responsible for the development of the separation zone in both the without submerged vane and with submerged vane experiments (Figure 8). The vertical velocities in the separation zone in the without submerged vane condition were lower ($w \approx 1m/s$) where significant sediment deposition occurred in this zone, whereas with submerged vane test case the velocities were greater ($w \approx 2m/s$), therefore the channel bed level was lower. The pattern of vertical vectors of cross-sections presents that a large curvature induced cell of helicalmotion exists in the inner side of the main channel. Curvature-induced secondary circulation is strongest slightly downstream of the intake channel entrance, commonly called the scouring zone (Herrero et al. 2015). The velocity distribution analysis in the cross section $X = [45, 55, 85]$ cm shows that the secondary circulation in the scouring zone causes strong scouring and that sediment material is carried from channel bed to the intake. Diversion of flow discharge provided by the intake to the main channel inevitably results in local flow acceleration downstream of the junction, and can be identified as a maximum velocity zone (seperation zone). Compared to the without vane system, the secondary flow pattern was markedly different and much weaker (Figure 8 and Figure 9). The distribution of stream-wise velocity is greater uniform for the with vane system than without. For without vane case, a large shift of accelerated high velocity flow from the inner side of the main channel toward the intake was observed (Figure 9). However, a less significant shift of flow was noticed for three-vane case. The contour plots of u_{yz} and vector arrows indicate that secondary flow was more strongly directed toward the inner side of the main channel and inside of the intake than in the three-vane case. It can be observed that three-vane case generates another secondary circulation around themselves before the intake entrance and this large withdrawal results in a highly complex three-dimensional flow field, reducing the stream-wise velocity component needed to produce a scour trench in front of the intake. Therefore, it can be concluded that the sediments are deposited after passing the intake and scouring occurs between the vanes. The large scour area was moved forward and a relatively narrow recirculation cell was formed just downstream of the intake mouth and along the inner side of the main channel. It was greater near the channel bottom, and prevented sediment entering the intake. The velocity distributions show that the vortex progressed continuously in a considerable distance downstream from the vanes (Figure 8 and Figure 9). The deposition area near the left side of the channel (Zone (2)), was also markedly reduced by moving sediment along to the channel downstream. The results were consistent with previous studies (Karami et al. 2017; Bajestan and Nazari 1999).

Strength of secondary flow

Previous studies showed that the strength of a secondary circulation depends upon the ratio of diversion flow velocity to the main flow velocity. With regard to Figure 9, the strength of the secondary flow is increased in the downstream corner of the intake in all cases. Also, Neary and Odgaard (1992) have reported that the maximum strength of the secondary flow formed at the downstream end of intake entrance (Subramanya and Awasthy 1972; Khashab and Smith 1976; Fares and Herbertson 1993; Agaccioglu and Yüksel 1998; Cosar and Agaccioglu 2004; Onen and Agaccioglu 2005; Emiroglu et al. 2010). There is a relationship between the strength of the secondary circulation and the velocity ratio. The strength of the secondary circulation δ inside of the channel can be expressed as Neary and Odgaard (1992):

$$\delta = v_s - v_b \tag{2}$$

where; δ is the strength of secondary circulation, v_s and v_b are transverse velocities measured near flow surface and bed surface, respectively. In this study, the dimensionless strength of secondary circulation δ/U' (where; U' is the average velocity of the main channel) was determined by the transverse velocities at the flow and bed surfaces in the intake channel at the coordinates of $x = 3.5$ m and $y = 0.00$ m. The dimensionless strength of secondary circulation δ/U' was calculated 0.90 under the velocity ratio of $log\,(u_2/u_1) = -0.13$ for without vane experiment (where; u_1 is the average velocity in main channel upstream of the intake, u_2 is the average velocity in the intake channel). Otherwise, the dimensionless strength of secondary circulation δ/U' was calculated 0.47 under the velocity ratio of $log\,(u_2/u_1) = -0.13$ for with vane experiment. It was noticed that the strength of secondary flow in the intake channel decreased by 48% with three vanes. The maximum strength of the secondary flow moved around the submerged vanes when used, thereby the strength of the secondary flow in the downstream corner of the intake is decreased. The diverted flow discharge provided by the entrance of the intake inevitably results in local flow acceleration downstream of the junction and can be defined as a maximum velocity zone (Figure 8 and Figure 9). Similar result was also reported in CFD numerical solutions by Karami et al. (2017).

The turbulence kinetic energy

As seen in Figure 10 vertical velocity components w in the separation zone caused relatively lower k values that observed under with submerged vane case. It is possible that it corresponds with the shear zone low velocity flow on the separation zone. The turbulent kinetic energy k started to increased after the intake entrance at the downstream of the main channel under without vane case, whereas k started to increased around the vanes under with vane case condition. The magnitude of k gradually decreased as it moved towards the water surface and was transported to downstream. The magnitude of k was also noticeably reduced for three-vane case (Figure 10). The near-bed streamlines were deflected by three submerged vanes towards the entrance of the intake channel, reducing the intensity. The accumulation of the streamlines at the tip of the vanes indicates the region of high shear layer. In the with vane experiments, the streamlines shifted toward the intake, and showed uniform low velocity in this zone, after passing the vanes. Compared to the without vane case, weaker turbulence close to the inner side of the main channel was caused by flow separation and high turbulence local pockets were observed for each vane, so high turbulence values were created and dispersed after passing through the intake mouth. The turbulence pockets related with the submerged vanes increased rapidly around the vanes. Significant turbulence occurs at the point where the relatively high flow from the main channel with respect to the side diversion channel mixes with the lower flow in the separation zone. This location of highly turbulent kinetic energies respect to the separation zone is similar for all diversion structures.

The width and length of the turbulent region in the main channel has a significant effect on the sediment entrance to the intake channel. The size of the turbulent region is related to the amount of sediment transport. In the test without vane, the experiment shows that secondary flow cell width of the turbulent region with $0.2b_m$ continued to a distance of $1.5b_m$ mount of the intake corner at the downstream side of the main channel is closely related to flow momentum. In front of the outer side of the main channel (Zone (2)), the formation of an external shear layer is defined by an increase in turbulence kinetic energy deposited sediment here. On the other hand, in the test with vane system, experiment shows that secondary flow cell width of the turbulent region with $0.15b_m$ continued to a distance of $0.5b_m$ mount of the intake corner at the downstream side of the main channel, which is only about $1/3$ of the result of the without vane experiment. k in scouring Zone (3) were very strong due to comparatively high velocity gradients at the corner of the intake mouth. By installing the three-vane, the flow was distorted from the intake toward the center line of the main channel. The location of the k was retracted from the downstream of the intake entrance to the location of the vanes after their installation. k was moved forward to the middle of the main channel, thus reducing its energy and increasing its flow characteristics. The distance of the turbulence from the intake toward to downstream of the main channel was found to be equal to 140 cm and 70 cm for without and with vane experiments, which corresponds to $2l_{k(with-vane)} = l_{k(withot-vane)}$ and $l_{k(with-vane)} = 4.7\delta_b$. The dimensions of the turbulent region was presented before by Karami et al. (2017) for open channel 90° bend with vanes. However, it has not been presented before, since sufficient experiments have not been done for water intake structures.

CONCLUSION

The influence of the submerged vanes on scour and deposition patterns in the 90° intake entrance is presented by the analysis of detailed bed topography and three-dimensional velocity measurements. The experiments were performed under movable bed conditions, and with continuous sediment feeding, which represents an innovation in the study of this type of intake structure. Three vanes with dimensions were; 10 mm thick, 3 cm high, 12 cm long, and aligned with $\alpha = 20°$ angle to flow direction installed in one column near the intake entrance. Based on the experiment results and analysis of data, the following main conclusions can be drawn: The results confirm the existence of a relationship between the hydrodynamics patterns and sediment transport. The observations showed that a second vortex formed parallel to the intake, next to the upstream slope of the scouring zone (Zone (1)) and it prevented movement of the sediment particles along the main channel downstream and it directed particles towards the intake. The recirculation zones (1), (2) and (4) were identified as the inner side of the main channel, before the intake and outer side of the main channel, opposite the diversion, respectively. Because of the low velocities, sediment was deposited in Zone (1) and Zone (2). The amount of sediment by 20% in the intake channel was reduced by 3 vanes in a single column and sediment transport in the main channel decreased by 125% under the mobile bed condition. The maximum scour occurred at the entrance corner of the intake in the downstream part of the main channel. In the three-vane experiment, maximum scour depth occurred around the tips of the vanes rather than of Zone (3). It can be concluded that local scour at the intake entrance can be reduced by submerged vanes. In the with vane conditions, sediment was transported faster along the main flume, and the intake took less sediment inside under sediment feeding. In addition, it was seen that the continuous sediment feeding to the main channel prevented bed armoring. The three-dimensional flow structure at a channel diversion generally conformed to accepted flow behavior in intakes. The three-vane case decreased the time-averaged velocity up to 45% at the mount of the intake corner at the downstream side (Zone (3)). The length and width of the scouring area which was observed just downstream from the intake mouth to downstream of the main channel was reduced by 15% and 50%, respectively, corresponding to 0 bed reference.

In experiments with submerged vanes, the vanes created tip vortices around them and changed the bed velocity profile. In without vane experiment, no longitudinal turbulence was detected prior to the diversion entrance. The turbulence started immediately after the entrance of the diversion channel. For this reason, the vanes were able to carry the sediment beyond the inlet channel by continuing the turbulent movement they started around themselves along the main channel. However, without vane experiments, the sediment coming from upstream of the main channel was directed directly into the water intake channel. k in scouring Zone (3) were very strong due to comparatively high velocity gradients at the corner of the intake mouth. By installing the three-vane, the flow was diverted from the intake toward the center line of the main channel. The location of the k was retracted from the downstream of the intake entrance to the location of the vanes after their installation. k was moved forward to the center line of the main channel, thus reducing its energy and increasing its flow characteristics. The distance of the turbulence from the intake toward to downstream of the main channel was found to be equal to 140 cm and 70 cm for without and with vane experiments, which corresponds to $2l_{k(with-vane)} = l_{k(withot-vane)}$ and $l_{k(with-vane)} = 4.7\delta_b$. In addition, the vanes increased the size of the separation zone defined in the intake channel compared to the without vane situation, while decreasing the sediment deposition in this region. The high turbulent kinetic energy region occurred just after the separation zone for the without vane case.

The results of the paper present the hydrodynamic effects of sediment transport of diversion. Experimental studies have investigated sediment control using submerged vanes, but the current study, in accordance with the literature, provides more extensive and thus more reliable experimental data, verifying presence of secondary motions both around the submerged vanes, and entrance of the intake as a result of flow separation. In addition, this paper emphasizes the importance of mobile bed condition caused by sediment feeding and indicates limitations of incipient motion, a situation rare in nature. The author recommends more experiments to better understand the complex sediment transport phenomena in intakes. To take this study one step further, the influence of submerged vane variables such as vane distances, vane angles or different intake ratios can be investigated. This paper is a good example for showing the limitations of experiments performed over a fixed bed and emphasizing the use of mobile beds to execute experiments. Further works are needed due to the flow pattern's direct influence on sediment transport to the intakes.

Acknowledgments

The author would like to special thank to Prof. Dr. Antonio Heleno Cardoso and Instituto Superior Tecnico (IST) Hydraulic Laboratory. The author would also like to thank Simon Edward Mumford for his help in language editing and proofreading.

Some or all data, models, or code that support the findings of this study are available from the corresponding author upon reasonable request.

437 **NOTATION**

438 *The following symbols are used in this paper:*

b	=	channel (river) width;
d	=	flow depth;
d_s	=	scour depth;
d_{50}	=	median grain size;
F_r	=	Froude Number;
g	=	gravitational acceleration;
H	=	submerged vane height;
k	=	turbulence kinetic energy;
L	=	submerged vane length;
Q	=	discharge;
q_r	=	discharge ratio;
t	=	time;
u_0	=	average approach flow velocity;
$\bar{u}_{xy}$	=	non-dimensional mean resultant velocity;
$\bar{u}_{yz}$	=	non-dimensional mean resultant velocity;
u, v, w	=	instantaneous velocity components;
$u' = u - \bar{u},$	=	fluctuating velocity component;
$v' = v - \bar{v},$	=	fluctuating velocity component;
$w' = w - \bar{w}$	=	fluctuating velocity component;
$\bar{u}, \bar{v}, \bar{w}$	=	mean velocity components;
$U',$	=	average velocity of the main channel;
$u_1,$	=	average velocity in the main channel upstream of intake;
$u_2,$	=	average velocity in the intake channel;
x, y, z	=	longitudinal, transversal and perpendicular to the channel bottom coord.;
X, Y, Z	=	distances in x, y, z directions, respectively;

α = vane angle of artack with flow;

δ = the strength of secondary circulation;

δ_n = vane spacing;

δ_b = distance from bank to vane; and

σ = geometric standard deviation.

Subscripts

i = intake channel; and

m = main channel.

REFERENCES

Barkdoll, B. D. 1997. Sediment control at lateral diversions. Ph.D. thesis, Iowa Institute of Hydraulic Research, University of Iowa, Iowa City, Iowa.

Bor, A. T. 2018. Experimental study of submerged vanes in intakes under sediment feeding conditions. E3S Web Conf., **40**, 03016.

Bulle, H. 1926. Untersuchungen über die geschiebeableitung bei der spaltung von wasserläufen. Berlin: VDI Verlag.

Odgaard, A. J. 2009. River Training and Sediment Management with Submerged Vanes. American Society of Civil Engineers.

Yang, F. 2008. Study on diversion angle effect of lateral intake flow. Journal of China Institute of Water Resources and Hydropower Research, **1**(8).

Abbasi, A. A. and MalekNejad, M. 2014. The effect of threshold and submerged vanes on sedimentary flow input to side basin. J. Irrig. Water Eng., **4**(16), 104–116.

Agaccioglu, H. and Yüksel, Y. 1998. Side-weir flow in curved channels. Irrig. Drain. Eng., **124**(3), 163–175.

Bajestan, S. and Nazari, S. 1999. The impression of the diversion angle of intake on the entering sediments to the lateral intakes at the vertical bond of river. J. Agric., Chamran University, **22**(1).

Cosar, A. and Agaccioglu, H. 2004. Discharge coefficient of a triangular side-weir located on a curved channel. Irrig. Drain. Eng., **120**(5), 410–423.

Davoodi, L. and Bejestan, M. S. 2012. Control of sediment entry to intake on a trapezoidal channel by submerged vane. Eco. Env. & Cons., **18**(1), 165–169.

Fares, Y. and Herbertson, J. 1993. Behaviour of flow in a channel bend with a side-overflow (flood relief) channel. Journal of Res., **31**(3), 383–402.

Goring, D. G. and Nikora, V. I. 2002. Despiking acoustic doppler velocimeter data. Journal of Hydraulic Engineering, **128**(1), 117–126.

Kasthuri, B. and Pundarikanthan, N. V. 1987. Discussion of "separation zone at open-channel junctions"; by james l. best and ian reid (november, 1984). Journal of Hydraulic Engineering, **113**(4), 543–544.

Keshavarzi, A. and Habibi, L. 2005. Optimizing water intake angle by flow separation analysis. Irrigation and Drainage, **54**(5), 543–552.

Khashab, A. and Smith, K. 1976. Experimental investigation of flow over side-weirs. Journal of Hydraulic Division, **102**(9), 1255–1268.

Lemmin, U. and Rolland, T. 1997. Acoustic velocity profiler for laboratory and field studies. Journal of Hydraulic Engineering, **123**(12), 1089–1098.

Neary, V. and Odgaard, A. J. 1992. Three-dimensional flow structure at open-channel diversions. Journal of Hydraulic Engineering, **119**(11), 4759.

Odgaard, A. J. and Kennedy, J. F. 1983. River-bend bank protection by submerged vanes. Journal of Hydraulic Engineering, **109**(8), 1161–1173.

Odgaard, A. J. and Spoljaric, A. 1986. Sediment control by submerged vanes. Journal of Hydraulic Engineering, **112**(12), 1164–1180.

Odgaard, A. J. and Wang, Y. 1991a. Sediment management with submerged vanes. i: Theory. Journal of Hydraulic Engineering, **117**(3), 267–267.

Odgaard, A. J. and Wang, Y. 1991). Sediment management with submerged vanes. ii: Applications. Journal of Hydraulic Engineering, **117**(3), 284–302.

Onen, F. and Agaccioglu, H. 2005. Clear-water scour at a side-weir intersection along the bend. Irrig. Drain. Eng., **54**, 553–569.

Potapov, M. V. and Pyshkin, B. A. 1947. Metod poperechnoy tsirkulyatsii i ego primenenie v gidrotekhnike. Izd. Ak. Nayk. SSSR: Moscow and Leningrad.

Subramanya, K. and Awasthy, S. C. 1972. Spatially varied flow over side weirs. Journal of Hydraulic Engineering, 1–10.

Amiri, S., Shoushtari, M. M., and Zadeh, H. H. 2013. Laboratory investigation effect of submerged vanes angle position with consideration distance ratio to govern inlet sediment to side intake structure at 180° degree bend. International Journal of Agriculture and Crop Sciences, **6**(18), 1292–1298.

Barkdoll, B., Hagen, B., and Odgaard, A. 1995. Sediment exclusion at hydropower intakes using submerged vanes. Journal of Hydraulic Engineering.

Barkdoll, B. D., Ettema, R., and Odgaard, A. J. 1999. Sediment control at lateral diversions: Limits and enhancements to vane use. Journal of Hydraulic Engineering, **125**(8), 862–870.

Biron, P., Roy, A., and Best, J. 1996. Turbulent flow structure at concordant and discordant open-channel confluences. Experiments in Fluids, **21**, 437–446.

Elci, S., Bor, A., and Caliskan, A. 2009. Using numerical models and acoustic methods to predict reservoir sedimentation. Lake and Reservoir Management, **25**(3), 297–306.

Emiroglu, M., Kaya, N., and H.Agaccioglu. 2010. Discharge capacity of labyrinth side weir located on a straight channel. Irrig. Drain. Eng., **136**(1), 37–46.

Herrero, A., Bateman, A., and Medina, V. 2015. Water flow and sediment transport in a 90° channel diversion: an experimental study. Journal of Hydraulic Research, **53**(2), 253–263.

Nakato, T., Kennedy, J. F., and Bauerly, D. 1990. Pump-station intake-shoalling control with submerged vanes. Journal of Hydraulic Engineering, **116**(1), 119–128.

Neary, V. S., Sotiropoulos, F., and Odgaard, A. J. 1999. Three-dimensional numerical model of lateral-intake inflows. Journal of Hydraulic Engineering, **125**(2), 126–140.

Sruthi, T. K., Ranjith, K. B., and Chandra, V. 2017. Control of sediment entry into an intake canal by using submerged vanes. AIP Conference Proceedings, https://doi.org/10.1063/1.4998378.

Weber, L. J., Schumate, E. D., and Mawer, N. 2001. Experiments on flow at a 90°; open-channel junction. Journal of Hydraulic Engineering, **127**(5), 340–350.

Beygipoor, G., Bajestan, M. S., Kaskuli, H., and Nazari, S. 2013. The effect of distance from submerged vanes to the intake at different angles of vanes on controlling the sediment entering the intake branching from a 90° convergent bend. International Journal of Farming and Allied Sciences, 591–598.

Guillén-Ludeña, S., Franca, M., Alegria, F., Schleiss, A., and Cardoso, A. 2017. Hydromorphodynamic effects of the width ratio and local tributary widening on discordant confluences. Geomorphology, **293**, 289 – 304.

Hassanpour, F., Ayoubzadeh, S., Ghoddasian, M., and Samani, G. V. 2007. Effect of submerged vanes on dewatering and longitudinal profile of water level in vicinity of 90-degree side basins. J. Dev. Nat. Resour, 104–114.

Karami, H., Farzin, S., Sadrabadi, M. T., and Moazenia, H. 2017. Simulation of flow pattern at rectangular lateral intake with different dike and submerged vane scenarios. Water Science and Engineering, **10**(3), 246 – 255.

Wang, Y., Odgaard, A. J., Melville, B. W., and Jain, S. C. 1996. Sediment control at water intakes. Journal of Hydraulic Engineering, **122**(6), 353–356.

List of Figures

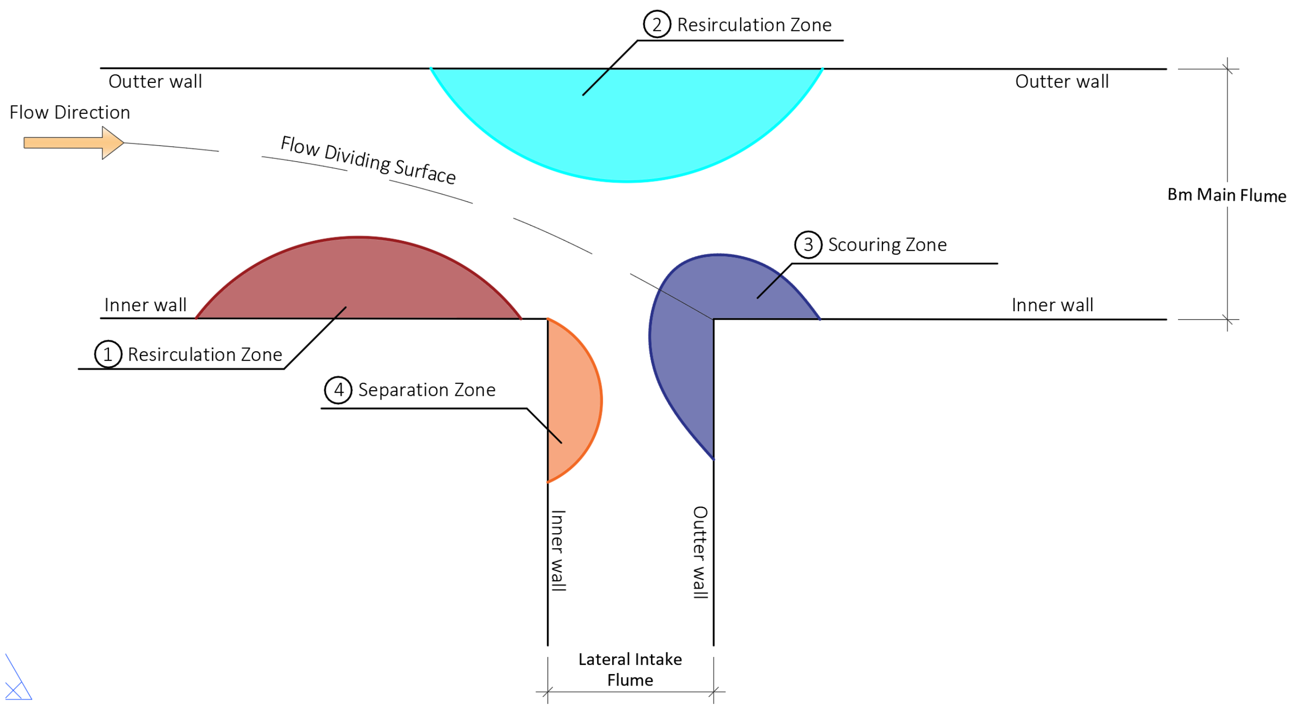

Fig. 1. Schematic diagram of intake scour and sedimentation areas

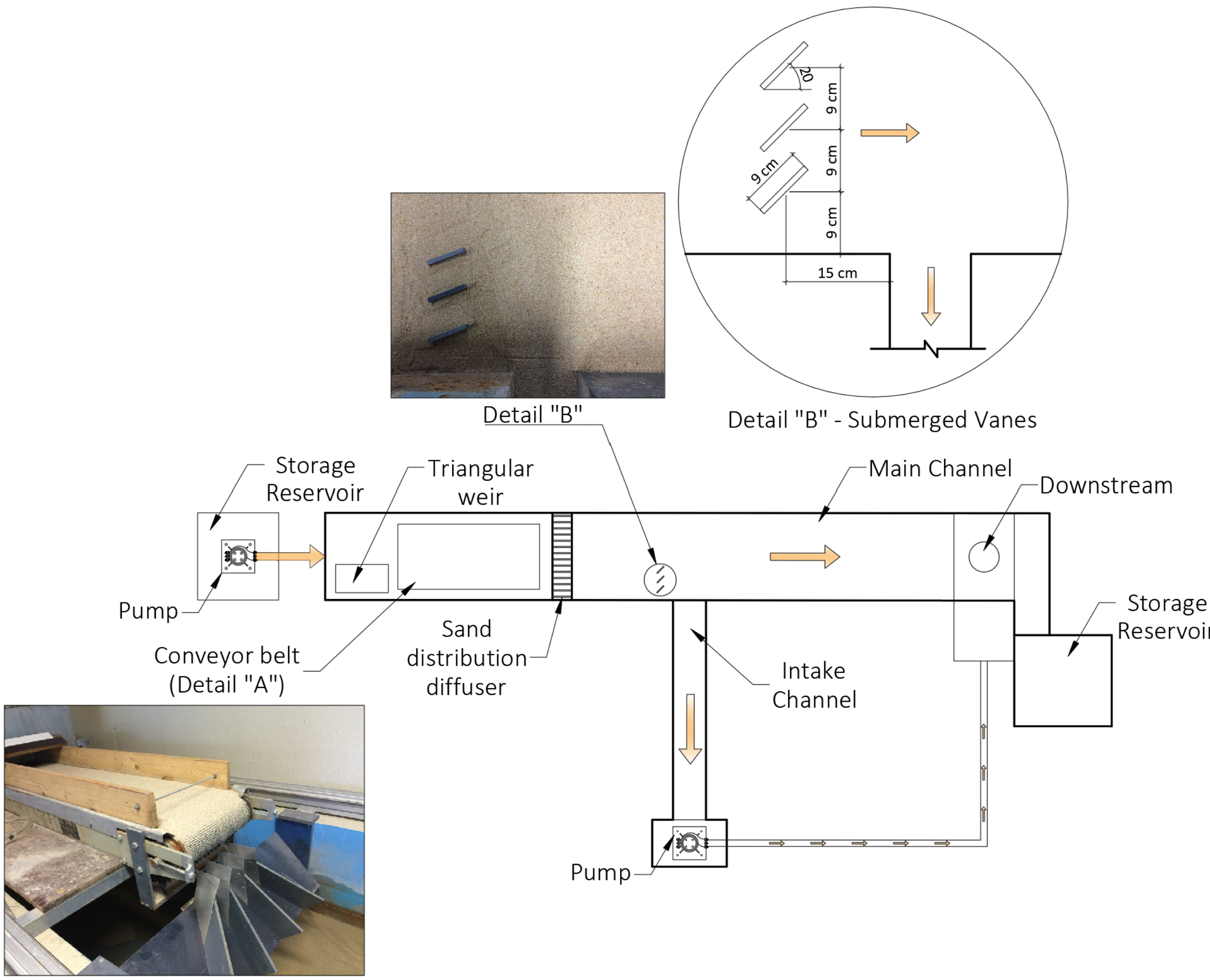

Fig. 2. Scheme of the experimental system (dimensions are in centimeters) a) Plain view b)Layout of the vanes (Bor 2018)

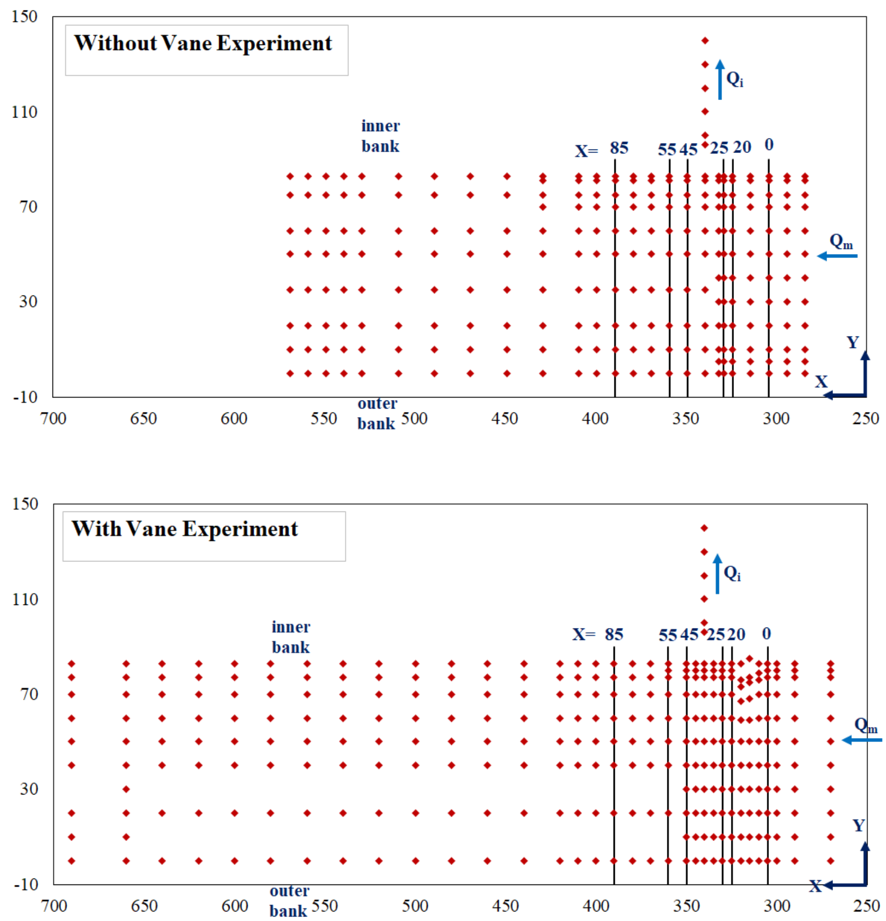

Fig. 3. The measurement velocity grids in plan view for without vane and with vane experiment (units are in centimeter)

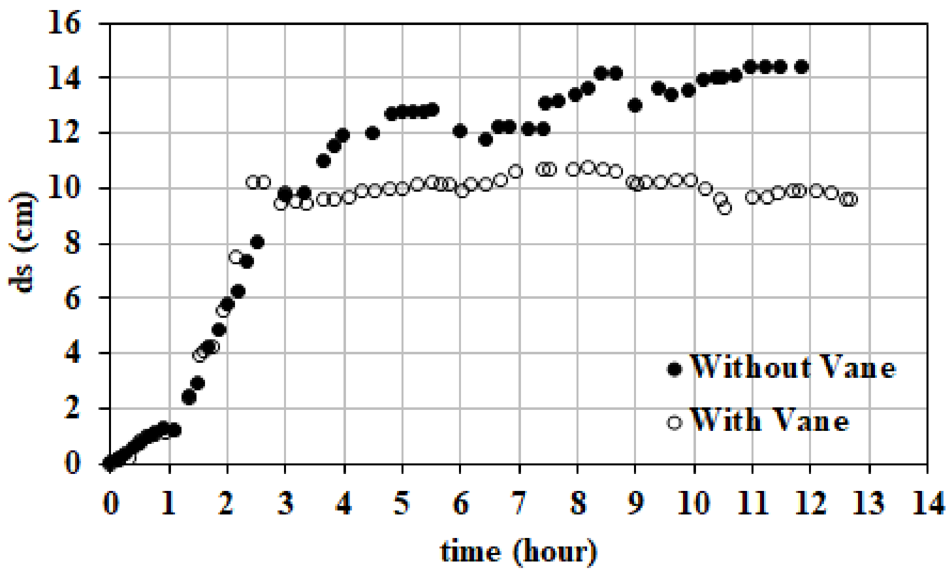

Fig. 4. Temporal variation of the scour depth at the corner of the intake upstream

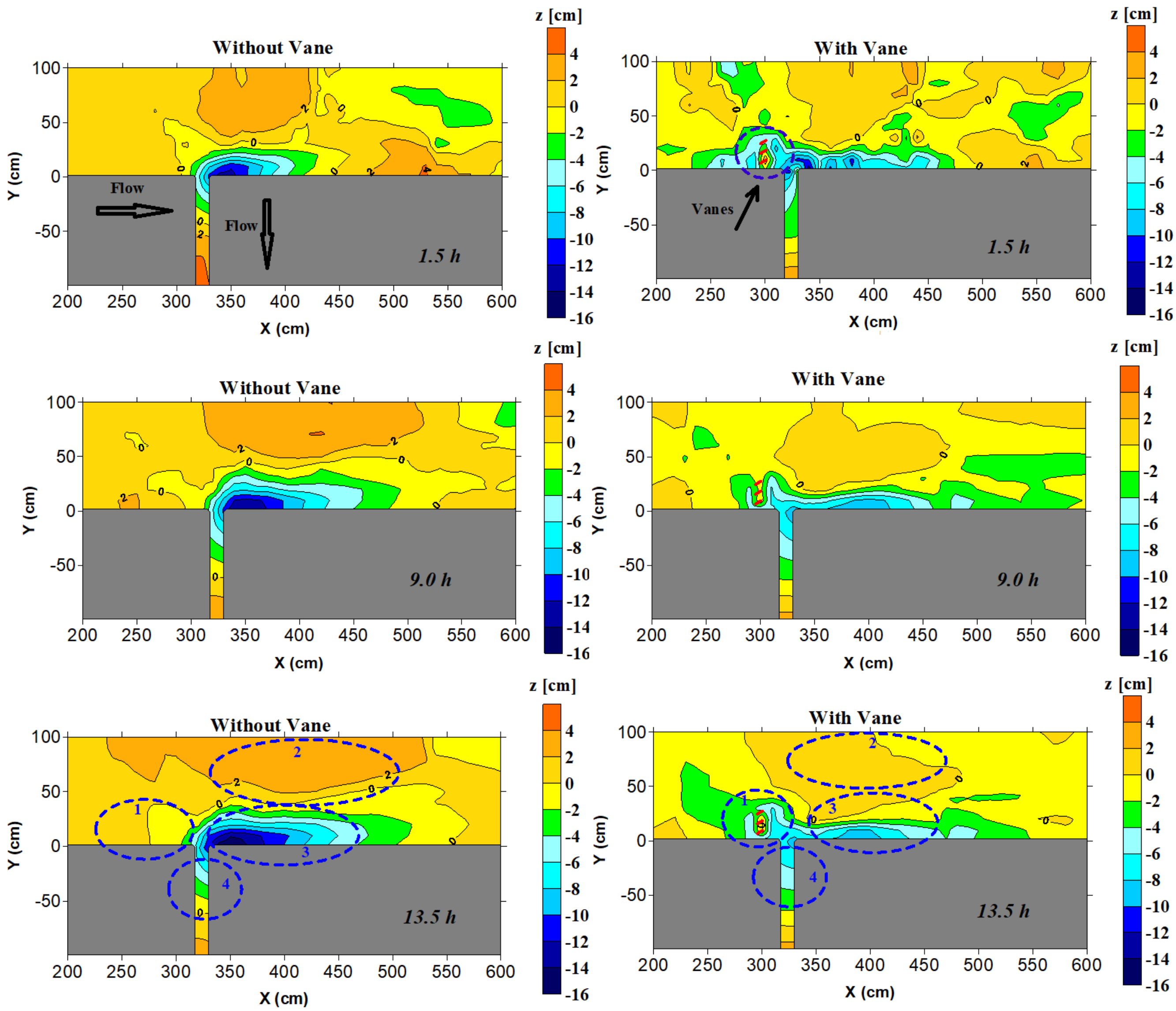

Fig. 5. Comparison of the bed topography

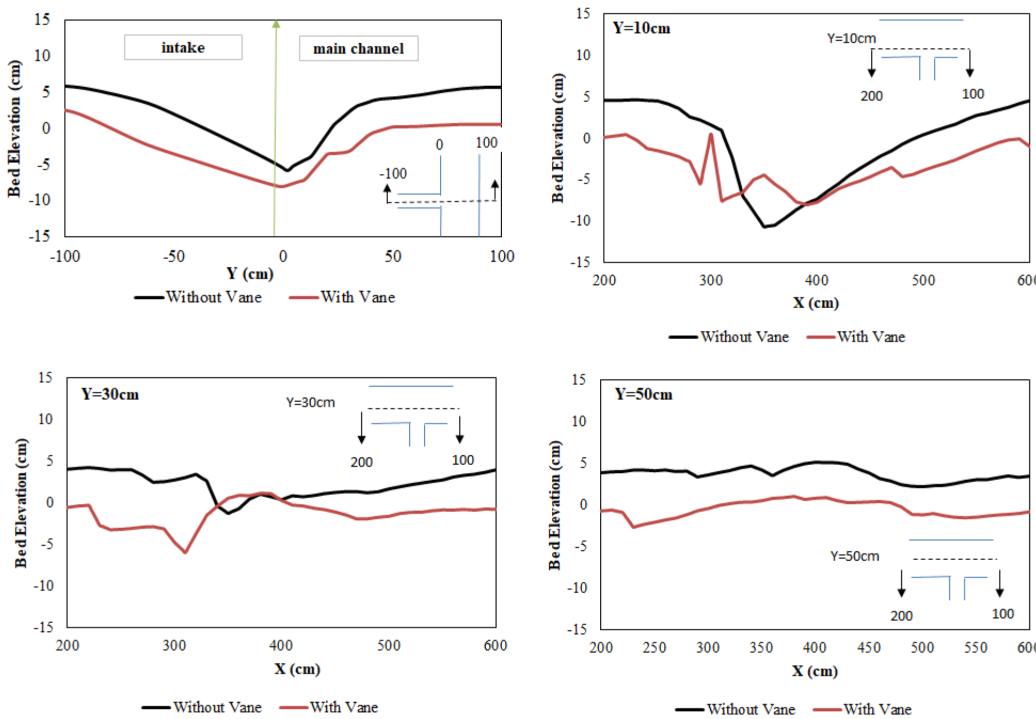

Fig. 6. Bed elevations along the centerline of the intake channel and Y=10 cm, Y=30 cm and Y=50 cm of the main channel at the end of tests

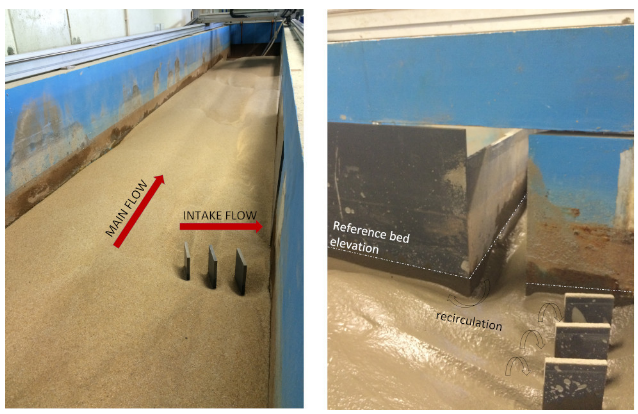

Fig. 7. The final topography configuration at the end of test

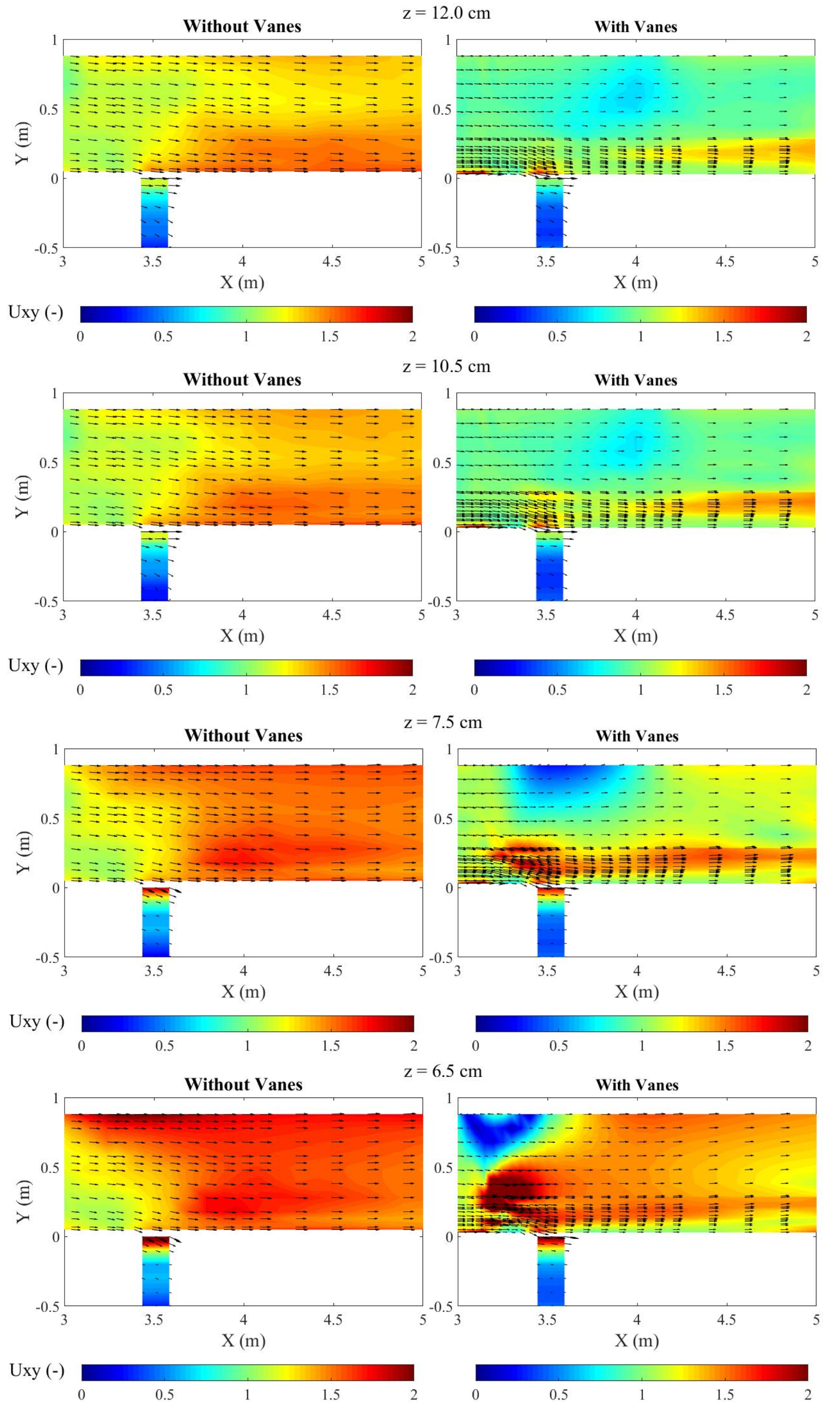

Fig. 8. Non-dimensional time-averaged velocity magnitude U_{xy} $(-)$ presented as colour scheme for horizontal planes at $z = 12cm$, $z = 10.5cm$, $z = 7.5cm$, and $z = 6.5cm$ above the bed. (vector arrows indicates direction of the velocity vector $\bar{u}_{xy}$)

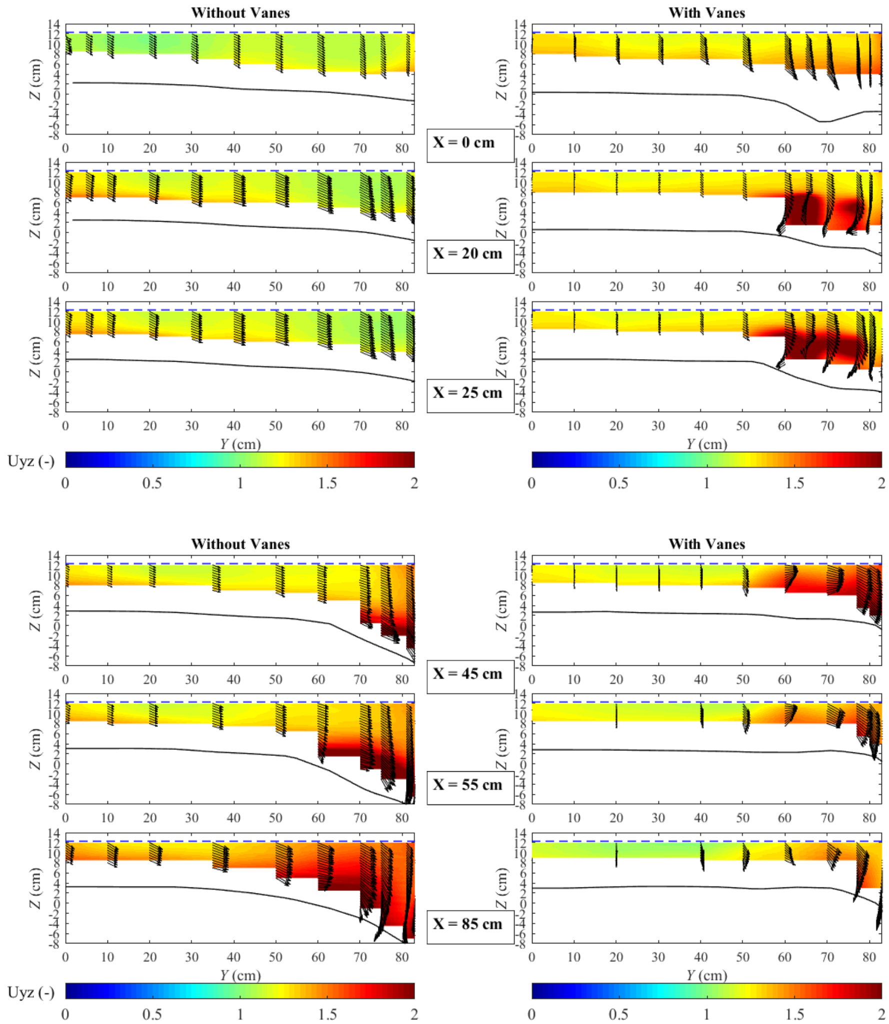

Fig. 9. Time-averaged mean velocities for the cross-sections $X = 0cm$; $X = 20cm$; $X = 25cm$; $X = 45cm$; $X = 55cm$; and $X = 85cm$. The colour scale shows $\bar{u}$ velocity and vector arrows show direction of $\bar{u}_{yz}$ on the yz plane. The blue dashed line indicates water surface elevation. The black continuous line represents the topography.

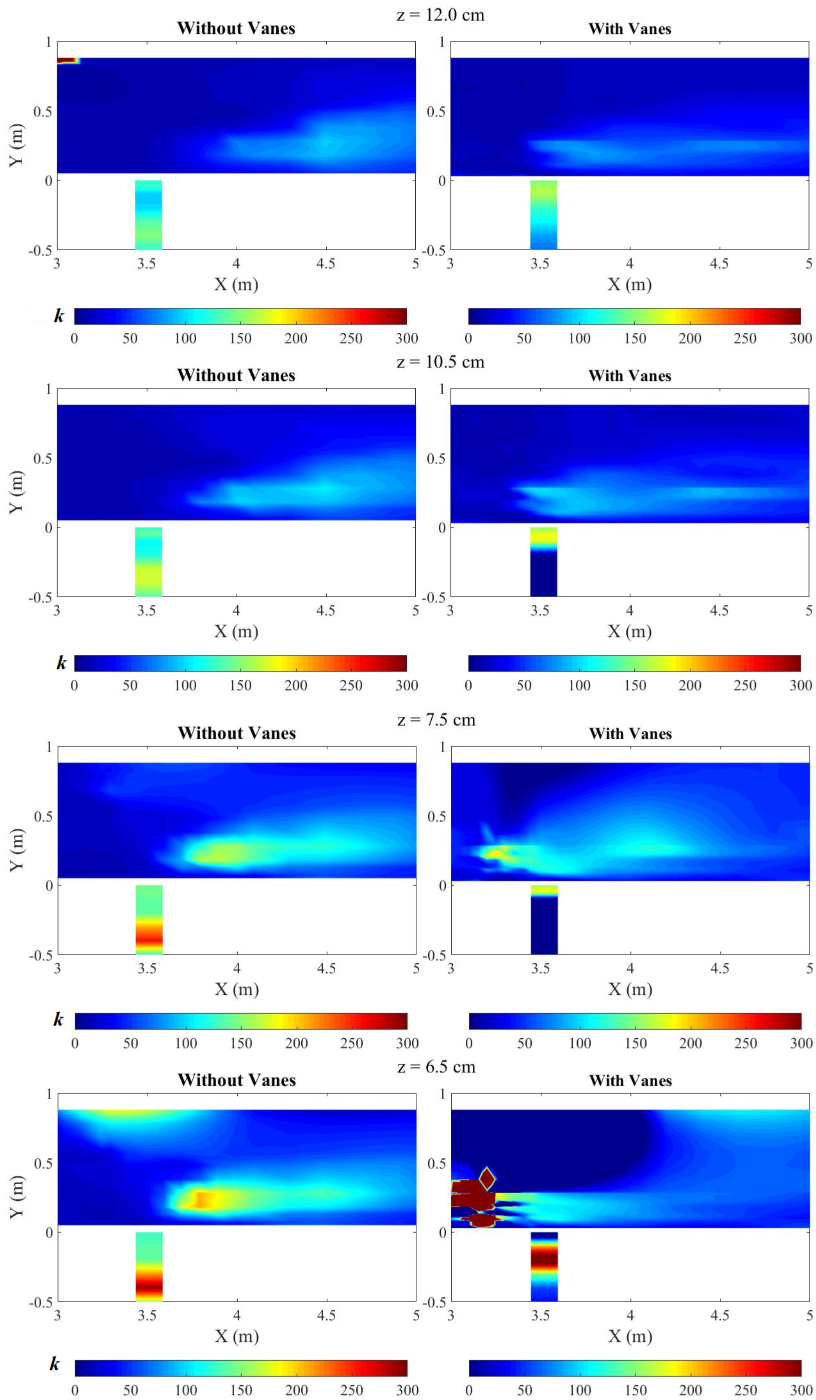

Fig. 10. Turbulence Kinetic Energy distributions k (cm^2s^{-2}) presented as colour scheme for horizontal planes at $z = 12cm$, $z = 10.5cm$, $z = 7.5cm$, and $z = 6.5cm$ above the bed.